Infrared Spectroscopic Study of Chemically lnduced Dewetting in Liquid Crystalline Types of Self-Assembled Monolayers

Yu-Tai Tao* and Wen-Ling Lin

Institute of Chemistry, Academia Sinica Taipei, Taiwan, Republic of China

Geoffrey D. Hietpas[†] and David L. Allara*[,†,‡]

Departments of Chemistry and Materials Science and Engineering, Materials Research Institute/Research Park, The Pennsylvania State University, University Park, Pennsylvania 16802

Received: August 1, 1997[⊗]

Self-assembled monolayers (SAMs) were prepared by chemisorption of *n*-hexadecanoic acid (**1**), 4-hexadecyloxybenzoic acid (**2**), and 4′-hexadecyloxybiphenyl-4-carboxylic acid (**3**), molecules with liquid crystalline properties, onto air-exposed silver substrates to produce films with essentially identical CO_2^-/Ag interfaces. Brief H_2S exposure leads to immediate $-CO_2H$ formation and film reorganization. Both the **1** and **2** SAMs dewet into discrete crystallites with their alkyl chain *c*-axes aligned near parallel to the substrate plane. In contrast, the **3** SAM reorganizes into a uniform, quasi-2-D, network of hydrogen-bonded CO_2H groups at the film/substrate interface in which the *c*-axes remain near perpendicular to the substrate plane. Upon extended storage in air, oxidation of the sulfided Ag surface layer induces a near complete return of the **1** SAM to its original state, while the **2** and **3** SAMs show only partial reversal. These results demonstrate the interplay between intermolecular and interfacial interaction forces and their effects on dynamic restructuring of highly organized monolayers under chemical stress.

1. Introduction

Self-assembled monolayers (SAMs) continue to receive considerable attention because of their scientific interest and potential applications such as chromatographic coatings, biosensors, and corrosion resistant coatings.[1] While it is generally expected that the strong substrate binding in many of these films will provide the requisite stability for many applications, recent studies have begun to focus on the actual instabilities which can be encountered and their relaxation mechanisms.[2,3] In fact, in some applications such as lithography,[4] controlled degradation of SAMs is highly desirable.

The issue of structural rearrangements induced in organic thin films under external stimuli has been a recent focus in our laboratories. In an initial report we showed that a sudden perturbation of a SAM on Ag by HCl exposure results in complete protonation of the carboxylate head groups with rapid dewetting of the film into discrete, highly oriented crystalline clusters of pure *n*-hexadecanoic acid.[2] In this case it was clear that the film intermolecular interactions were insufficient to prevent formation of the crystallites. In the present report we now extend these studies by examining the effects of changing the intrinsic chemical structure of the adsorbate molecule on the film instability. For this purpose we have chosen liquid crystalline (LC) types of molecules which are well-known to be very efficient at self-assembling into a variety of structural phases. Further, the wetting behavior of LC molecules at oxide interfaces is of significant interest[5] because of the relevance to applications such as LC displays where alkyl-substituted aromatic molecules are assembled at transparent oxide electrodes.[6] With this in mind, we initiated an investigation of the effects of incorporating phenyl substituents into SAM molecules and now report on a series of monolayers on Ag made from self-assembly of *n*-hexadecanoic acid (**1**), 4-hexadecyloxybenzoic acid (**2**), and 4-hexadecyloxybiphenyl-4′-carboxylic acid (**3**). The structure of the initial SAM from **1** has been previously characterized in detail,[7] and qualitative aspects of the initial SAM from **3** have been reported.[8] To induce a sudden chemical perturbation of the monolayer interfaces, we have used H_2S, which is well-known to be very aggressive in forming a sulfided surface on the Ag substrate yet remains completely unreactive with the constituent acids of the SAM. Further, the effects of H_2S on these films is of great practical interest because of the long-standing issue of ubiquitous sulfide tarnishing of the surfaces of silver and its alloys by atmospheric exposure,[9,10] a problem that can be expected to arise in applications of SAMs on Ag involving typical ambient environments. In a previous study on *n*-alkanoic acid-based SAMs, we reported on the destabilizing effects of HCl, another aggressive agent for Ag surfaces.[2] The use of a *n*-hexadecanoic acid SAM in the present study allows a direct comparison of the effects of HCl and H_2S. Overall, while we find that the two gases exhibit quite similar but not identical effects, we have chosen the focus to be on H_2S because of its greater relevance to the general issue of environmental stress. Our results show profound effects of changing the intrinsic molecular structure on the H_2S-induced reconstruction of the SAMs. In particular, while the SAMs from **1** and **2** dewet into discrete, highly oriented crystallites of the initial acids upon H_2S exposure, the addition of the extra phenyl ring in compound **3** leads to a striking shift in the structural relaxation to a continuous monolayer with a hydrogen-bonded, CO_2H headgroup network. These results show the delicate balance between the intermolecular packing forces in the SAMs and in the bulk crystal phases of the constituent molecules and the energetics of the substrate/SAM interface.

2. Experimental

Materials. The *n*-alkanoic acids were obtained from Merck and The Tokyo Chemical Industry. Samples of 4-hexadecy-

[†] Department of Chemistry.
[‡] Department of Materials Science and Engineering.
[⊗] Abstract published in *Advance ACS Abstracts,* October 15, 1997.

S1089-5647(97)02514-5 CCC: $14.00

loxybenzoic acid and 4-hexadecyloxybiphenyl-4′-carboxylic acid were prepared by alkylation of corresponding 4-hydroxy-substituted acids using established procedures.[11] All of the acids were recrystallized several times from ethanol and gave the expected NMR and IR spectra. Sharp melting points of (**1**), 62.8;[12] (**2**), 132.5; and (**3**), 236.9 °C were observed. The melting points of **2** and **3** were obtained from DTA measurements, which were also used to verify the liquid crystalline nature of these molecules. Smectic-C transitions were found for **2** and **3** at 101.5 and 153.8 °C, respectively. Hexadecane was dried by percolation through activated alumina. Anhydrous hydrogen sulfide (99%) was obtained from Aldrich. Silver metal (99.99+%) was obtained from Johnson Matthey.

Monolayer Preparation and Characterization. The Ag substrates were prepared by vacuum deposition onto 2 in. silicon wafers using established procedures.[13] Monolayers were prepared by self-assembly from 0.25 mM hexadecane/THF (1:1 v/v) solutions as described previously.[8] Film thicknesses were determined by single-wavelength ellipsometry (632.8 nm and 70° angle of incidence) using a real refractive index of 1.5. Contact angles were measured on a Rame-Hart NRL Model 100 goniometer using hexadecane and purified water as probe liquids. Infrared reflection spectra (IRS) were obtained using published methods and are reported as $-\log(R/R_0)$ where R and R_0 are the reflectivities of the film-covered sample and a clean gold-coated reference wafer, respectively.[13] Complex refractive index (optical function) spectra, $\hat{n}(\tilde{\nu}) = n(\tilde{\nu}) + ik(\tilde{\nu})$, where $\tilde{\nu}$ is the wavenumber, of the bulk compounds were obtained from transmission spectra of KBr dispersions, as described elsewhere.[14] Orientational analysis of the monolayer film structures was performed by best-fit spectral simulation procedures.[14] Optical functions were not obtained for bulk carboxylate salts, e.g., Ag salts, since these always appeared significantly more disordered than the corresponding SAMs and thus provide poor models for simulations of the SAM spectra.

H_2S Exposure. The monolayer was placed in an airtight chamber flushed thoroughly with high-purity nitrogen. The H_2S was introduced with a syringe to create a partial pressure of 0.01 atm. After l min exposure, the samples were removed and periodically analyzed. Between analyses, the samples were maintained in clean wafer containers sealed under an ambient atmosphere. The 1 min. exposure was taken as a standard condition since this time was found to result in full disruption of the SAM−Ag interface without visible corrosion of the Ag surface. Small variations of this time had no effects on the reorganization behavior of the SAMs. In all cases, the H_2S-treated surfaces did not exhibit any visible corrosion, even after extended ambient exposure, in contrast to the behavior of HCl-exposed SAMs.[2] In general, it can be expected that for the concentration and short H_2S interaction times used here the thickness of the sulfided layer is less than ∼5 Å.[9]

3. Results and Analysis

3.1. The *n*-Hexadecanoic Acid (1) SAM. *3.1.1. Pre-H_2S Structures.* The initial **1**-SAM shows an ellipsometric film thickness of a 21.7 ± 0.5 Å with advancing water and hexadecane contact angles of 111 ± 1° (∼6° hysteresis) and 52 ± 1° (∼1° hysteresis), respectively, in agreement with previous reports.[2,7]

The IRS spectra, before and after H_2S exposure, are shown in Figure 1. The high-frequency region is shown in greater detail in Figure 2. A summary of the IR-active modes observed in the SAM films and in the polycrystalline bulk phases is given in Table 1 for all of the molecules studied in this report; the top of the table also shows the chemical structures of the

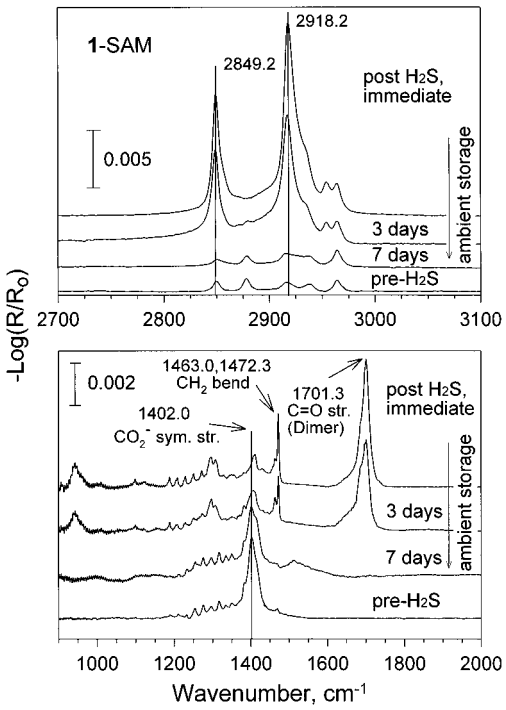

Figure 1. IRS spectra of a *n*-hexadecanoic acid (**1**) SAM on Ag. The spectra were taken before and after exposure to H_2S, as indicated.

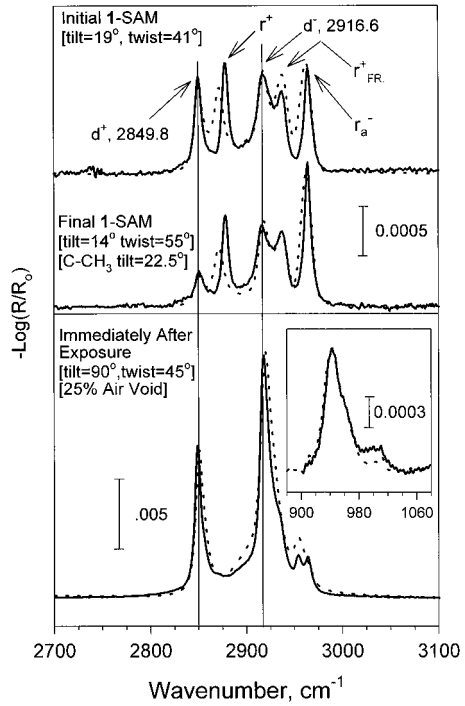

Figure 2. C−H stretching region IRS spectra of a **1**-SAM on Ag. Top: Initial SAM and final film after H_2S exposure and extended ambient storage. Bottom: immediately after H_2S exposure.

molecules. As expected, the spectrum of the initial **1**-SAM is identical to that published previously.[2] The detailed monolayer structure derived in the earlier report consists of highly trans-conformation chains attached to the substrate via $-CO_2^-$ groups and tilted slightly away from a normal surface orientation. A simulation analysis of the present C−H stretching spectral region, based on the reported optical function spectra of **1**,[2] results in the average chain orientational characteristics summarized in Table 2, essentially identical to those reported earlier. The definition of the chain axis tilt and C−C−C plane twist

TABLE 1: Band Assignments for Selected Vibrational Modes of Molecules 1, 2, and 3 in Initial SAMs and Pure Bulk Phases

	$C_{16}H_{33}CO_2H$ (**1**)		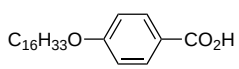 (**2**)		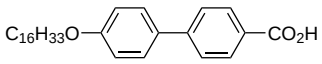 (**3**)		
mode	bulk	SAM	bulk	SAM	bulk	SAM	ref
asym. CH_3 str. (r_a^-)	2962.7	2963.6	2969.2	2964.6	not obsvd.	2964.7	2
asym. CH_3 str. (r_b^-)	2953.8	not obsvd.	2954.9	not obsvd.	2954.4	not obsvd.	2
sym. CH_3 str. (r_{FR}^+)	not obsvd.	2938.1	2932 sh.	2936.6	2935.5	2936.6	2
antisym. CH_2 str. (d^-)	2915.9	2916.6	2917.4	2918.9	2917.3	2920.1	2
sym. CH_3 str. (r^+)	2871.4	2877.8	2871.8	2877.8	2873.4	2878.5	2
sym. CH_2 str. (d^+)	2848.4	2849.8	2849.3	2850.7	2848.9	2851.4	2
CH_2 bend (γ_{CH_2})	1463.3, 1472	~1469.8	1469.5	1464.3, 1474.6?	1464.3, 1472.1	1464.5, 1475.3	29
OH str. (ν_{OH}^{dimer})	2250−3250	not obsvd.	2250−3350	not obsvd.	2200−3450	not obsvd.	27
C═O dimer str. ($\nu_{C=O}^{dimer}$)	1684.5, 1701	not obsvd.	1671.7, 1689.7	not obsvd.	1686.6, 1708.3, 1726.1	not obsvd.	26
sym. CO_2^- str. [$\nu_s(CO_2^-)$]	not obsvd.	1402, 1411 (sh)	not obsvd.	1394.4	not obsvd.	1392.7, 1398.3	7
antisym. str. [$\nu_a(CO_2^-)$]	not obsvd.	not obsvd.	not obsvd.	not obsvd.	not obsvd.	not obsvd.	15
OH bend op (γ_{OP}^{dimer})	942.0	not obsvd.	942.6	not obsvd.	920.3, 943.0	not obsvd.	27
C═C tang. str. (ν_{8a})			1607.0	1608.6	1604.6	1604.6	21, 22
C═C tang. str. (ν_{8b})			1579.1	1588.0	1582.9	1584.5	21, 22
C═C str. (ν_{19a})			1513.9	1510.7	1530.3	1528.2	21, 22
C═C str. (ν_{19b})			1432.8	not obsvd.	1435.9	not obsvd.	21, 22
aryl C−O str. [ν(Ar−O)]			1258.6	1258.6	1258.5	1259.5	22
aryl C−H op. (ν_{17b})			846.3	not obsvd.	837.0	847.1	21, 22
C═C radial str. (ν_1 or ν_{12})			771.8	not obsvd.	773.1	not obsvd.	21, 22

TABLE 2: Average Molecular Orientation of SAMs, before and Immediately after H_2S Exposure, Determined from Spectral Simulation Analysis. The Orientation Angles Are Defined in Figure 3

		molecule					
		$C_{16}H_{33}CO_2H$ (**2**)		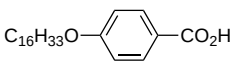 (**2**)		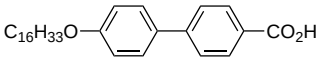 (**3**)	
tilt (θ) and twist (ψ) for selected groups, deg	diagnostic mode(s) used	initial SAM	H_2S exposed[a]	initial SAM	H_2S exposed[b]	initial SAM	H_2S exposed[c]
θ(chain)	d^+, d^-	19 ± 1	90 ± 10	38 ± 1	90 ± 1	37 ± 1	52 ± 3
ψ(chain)	d^+, d^-	42 ± 2	45 ± 2	38 ± 2	75 ± 2	41 ± 2	45 ± 2
θ(−C_6H_4− axis)	ν_{8a}			~0[d]	75 ± 2	~0[d]	35.5 ± 2
ψ(−C_6H_4− axis)	ν_{17b}				32 ± 4		36 ± 4
ψ(CO_2H dimer ring plane)	γ_{OP}^{dimer}	*e*	45 ± 2	*e*	32 ± 4	*e*	*f*
θ(CO_2H dimer O−H axis)	ν_{OH}^{dimer}	*e*	>70°	*e*	>70°	*e*	36 ± 4[g]

[a] Discrete crystallite, 25% void model; see text. [b] Discrete crystallite, 80% void model; see text. [c] Continuous film model; see text. [d] Orientation set by the absence of the ν_1 and ν_{17b} modes. Simulation analysis was not utilized because the ν_{8a} optical function of the carboxylate SAM is not accurately described by that of the bulk carboxylic acid. For details see text. [e] Not observed. Indicates complete dissociation of the $-CO_2H$ groups in the SAM films. [f] Not observed. Taken as an indication that CO_2H dimers are not formed. [g] The broad O−H str. mode was used to make a rough estimate of the average O−H bond orientation.

angles for an all-trans chain is shown schematically in Figure 3A. For reference, the resultant best-fit simulation is given in Figure 2.

In the low-frequency region (Figure 1), there is a strong symmetric $-CO_2^-$ stretching mode [$\nu_s(CO_2^-)$] near 1400 cm^{-1}. This observation together with the absence of the companion antisymmetric stretching mode [$\nu_a(CO_2^-)$], typically observed near 1510 cm^{-1} in asymmetrically bound SAMS,[15] is consistent with a C_{2v} symmetry $-CO_2^-$ species, attached in a bidentate fashion to the substrate with both O atoms at the surface plane.[2,16] Because of the lack of a reliable value for the $\nu_s(CO_2^-)$ transition dipole moment magnitude, the data do not allow determination of the C_{2v} axis tipping angle relative to the surface. A cartoon representation of the average chain structure is given in Figure 4. The exact configuration of the CO_2^- group is not shown since the tipping angle is unknown.[17]

3.1.2. Post-H_2S, Immediate Analysis. Immediately after H_2S exposure, a dramatic restructuring of the monolayer assembly results. The water contact angle decreases from 111° to near 70° with substantially increased hysteresis, while hexadecane completely wets the surface. These changes parallel the reported effects of HCl exposure.[2]

The IRS spectra (Figures 1 and 2) are nearly identical to those reported earlier for the HCl-exposed SAM, and thus it can be concluded that two films are quite close in structure. Our previous analysis showed this general structure to consist of discrete monoclinic crystallites of **1** with the *c*-axes oriented nearly parallel to the substrate, thus placing the (010) or (100) crystal surface planes in contact with the substrate. Within the crystallites, the molecules exist in the form of acid dimer rings with the chains in all-trans forms and packed in orthorhombic subcells with a 90° setting angle between adjacent chain C−C−C planes. Spectral simulation analysis of the present data (Figure 2 bottom, dotted line), following the earlier procedure,[2] shows that the H_2S-induced crystallites possess an average height of ~33 ± 5 Å and are distributed on average with a 28 ± 5% void content between them. The overall results of the analyses are summarized in Table 2, and a cartoon representation is given in Figure 4. For comparison, the HCl-induced reorganization was reported to result in a similar average crystallite size of ~50(±7) Å.[2]

3.1.3. Post-H_2S, Extended Ambient Exposure. Upon extended ambient exposure of the H_2S-treated sample, gradual changes were observed in the characteristics and after ~3−7

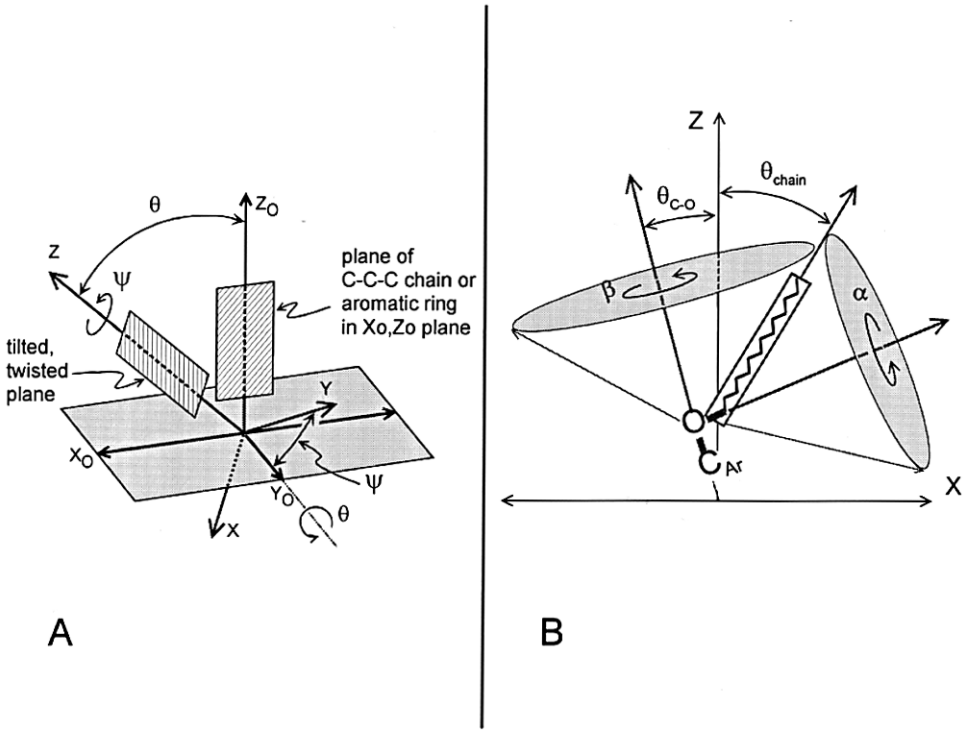

Figure 3. (A) Coordinate diagram defining the tilt and twist angles (θ, ψ) of the hydrocarbon C−C−C (long axis) and aromatic ring (1,4 para-axis) planes from the surface normal. (B) Bond rotation angles α and β defining rotation about the $C_{AR}O-CH_2$ and $C_{AR}-O$ bonds, respectively.

days (typical sample to sample variation) a final state resulted that was similar to the original SAM. The recovery indicates that upon air exposure an oxide layer returns on the Ag and induces a reversal of the film back to a form approaching the original SAM. The final water contact angle of 109 ± 2° is identical within error to that of the original SAM but shows a greater hysteresis (∼20° vs 6°). As a detailed test of structural changes, a companion SAM of *n*-$C_{14}H_{29}CO_2H$ was prepared and the hexadecane contact angles were examined for typical odd−even chain length effects on the wetting. The initial values of 52 ± 1° and 46 ± 1° for the **1** and the odd chain SAM were observed to merge to 51° and 50°, respectively, in the recovered films. This change, together with the increased hysteresis values can be taken as an indication of a slight "roughening" of the $-CH_3$ surfaces, which degrades the molecular-scale, odd−even topographical structure differences. These effects are different than those reported for the HCl exposure case, where a near complete return of the odd−even wetting effect was observed in the recovered films.[2]

The final IRS spectra are roughly similar to those of the previous HCl case. For the latter, the air exposure data were interpreted in terms of a return of the original ambient Ag oxide surface via oxidative degradation of the chloride overlayer with a subsequent overall breakup of the RCO_2H crystallites back to a structure nearly identical to that of the original SAM.[2] However, close examination of the spectra in Figures 1 and 2 shows some features that indicate an incomplete return to the original structure in the H_2S case. It is likely that this is caused by a failure of the sulfided Ag surface to return completely to the identical, original ambient oxide state under our exposure conditions.

First, the low-frequency spectra (Figure 1) indicate differences in the CO_2^- structure relative to the original SAM. In particular, the presence of a 1411 cm^{-1} shoulder on the main ν_s (CO_2^-) peak at 1401 cm^{-1} (compare pre-H_2S and 7 days spectra) indicates the presence of a second CO_2^-, headgroup species, with a frequency similar to that observed for species formed by chemisorption of CH_3CO_2H from the vapor[18] or solution.[19] Further, in contrast to the initial SAM, the $\nu_a(CO_2^-)$ mode becomes visible at 1510.8 cm^{-1}. This indicates that the headgroup geometry has shifted, on average, to a tipped configuration in which the axis through the O atoms is lifted away from the surface, i.e., toward a monodentate type of binding.

Second, one can note in Figures 1 and 2 definite decreases in the d^+ and d^- intensities (at ∼2850 and 2917 cm^{-1}, respectively). A simulation analysis reveals a decreased chain tilt of 14 ± 1° in the recovered film (simulation spectrum shown as dotted line in Figure 2, top). It is interesting to note that this structure is similar to that of *n*-alkanoic acid SAMs on ambient copper, where the chains are more vertical than on Ag and the CO_2^- headgroups exhibit a tipped binding geometry.[2] In the present case however, since the pre-H_2S SAM exhibits a higher tilt of 19°, the 5° decrease following H_2S exposure implies that the area per chain has decreased and thus that a small fraction of voids must arise upon exposure. Finally, note that the CH_3 r_a^- mode (2964 cm^{-1}) is noticeably intensified relative to the initial SAM spectrum. This increase is reminiscent of the relative increases observed between odd and even chain-length films. These changes arise because of alternation in the $C-CH_3$ surface orientation. The appearance of such changes in the CH_3 group orientation after H_2S exposure confirms the conclusions of disrupted film topography arrived at from the wetting angles and chain orientation data above.

3.2. The 4-Hexadecyloxybenzoic Acid (2) SAM. *3.2.1. Pre-H_2S Structure.* The initial film shows an ellipsometric thickness of 22 ± 1 Å and exhibits water and hexadecane contact angles of 110 ± 2° and 52 ± 2°, respectively. These values are consistent with a well-formed, CH_3-terminated monolayer.

For reference in discussing the IRS data, the spectrum of bulk **2** is shown in Figure 5 in the intrinsic form of $k(\tilde{\nu})$, the imaginary part of the complex optical function.[20] Selected mode assignments relevant to the analysis below are given in Table 1. For the orientation analysis of the **2**-SAM structures, in addition to the C−H and CO_2H group modes used for the **1**-SAM case,

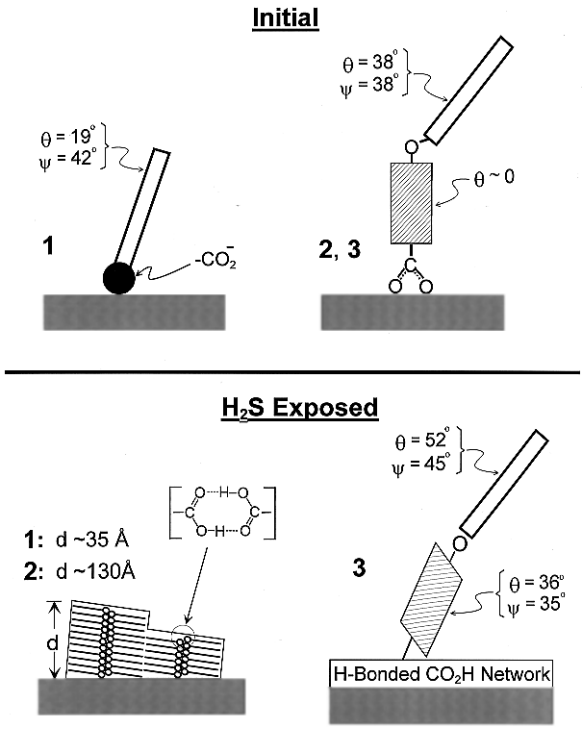

Figure 4. 4. Cartoon representations of the average molecular structures in the **1**-, **2**-, and **3**-SAMs before and immediately after H_2S exposure. The angles shown are taken from Table 2, and the coordinates are defined in Figure 3. In all cases, the intital SAMs consist of a uniform monolayer of molecules bound to the surface by symmetrical CO_2^- groups with their O atoms adjacent to the substrate surface. The H_2S-exposed **1**- and **2**-SAMs dewet into nanometer-scale crystallites dispersed across the surface with the average dimensions shown (*d*). The crystallites consist of dimeric species linked by acid dimer rings with the long axes of the aromatic rings and the chains close to parallel to the surface. The C−C−C planes are close to parallel to the surface, while the aromatic ring planes are oriented more toward edge-on to the surface (not shown). The **3**-SAM maintains a uniform monolayer structure after H_2S exposure, but the $-CO_2^-$ headgroup layer is converted to a complex H-bonded network of $-CO_2H$ groups. Group orientations are summarized in Table 2.

three specific aromatic ring modes were particularly useful: (1) a −C═C− tangential stretch (ν_{8a}, ∼1607 cm^{-1}) with a transition electric dipole moment vector (**p**) parallel to the 1,4 axis of the para-substituted benzene ring,[21] (2) a radial skeletal stretching mode (ν_1, 772 cm^{-1}) with **p** along the radial axis (in the aromatic ring plane and perpendicular to the tangential axis),[22,23] and (3) the out-of-plane (op) bending mode (ν_{17b}, 840 cm^{-1}) with **p** normal to the ring plane.[21,22] The assignments are summarized in Table 1, and further descriptions of the modes can be found elsewhere.[24]

The spectrum of the initial SAM is given in Figures 6 and 7. It is considerably more complex than the **1**-SAM spectrum in the low-frequency region because of the presence of the aromatic modes. However, the ν_s (CO_2^-) headgroup mode can be observed clearly (Figure 6 bottom), and its close correspondence to the **1**-SAM case (near 1394 and 1401 cm^{-1}, respectively), together with an apparent absence of the ν_a (CO_2^-) mode, indicates that the headgroup binding in the two SAMs is virtually identical.

The absence of the low-frequency ν_1 and ν_{17b} radial and op modes in Figure 6 clearly indicates that the aromatic ring plane is nearly orthogonal to the surface plane. However, simulation analysis of mode ν_{8a} results in the best fit, shown in Figure 8, which corresponds to a ring tilt of 41.5 ± 1°. For comparison, a completely orthogonal ring (in which the 1,4 para-substituted axis is perpendicular to the substrate) would show an intensity

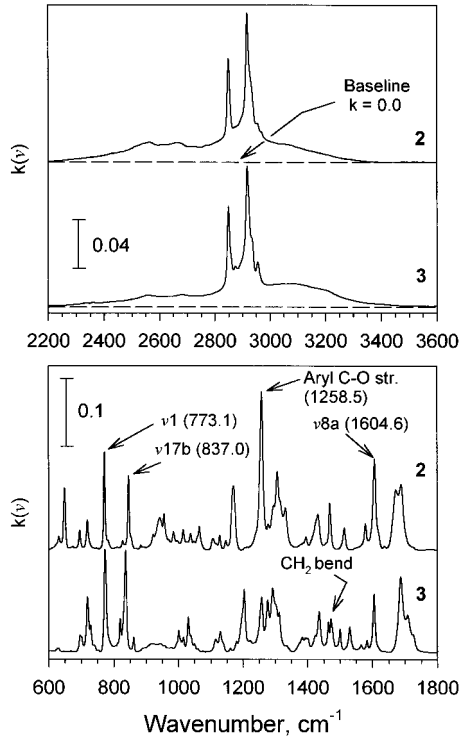

Figure 5. Isotropic absorption coefficient spectra (*k* spectrum) of the bulk polycrystalline phases of hexadecyloxy aromatic acids **2** and **3**. The dashed lines indicate the baseline for zero absorption. Top: high-frequency region. Bottom: Low-frequency region which contains the aromatic and carbonyl absorption regions.

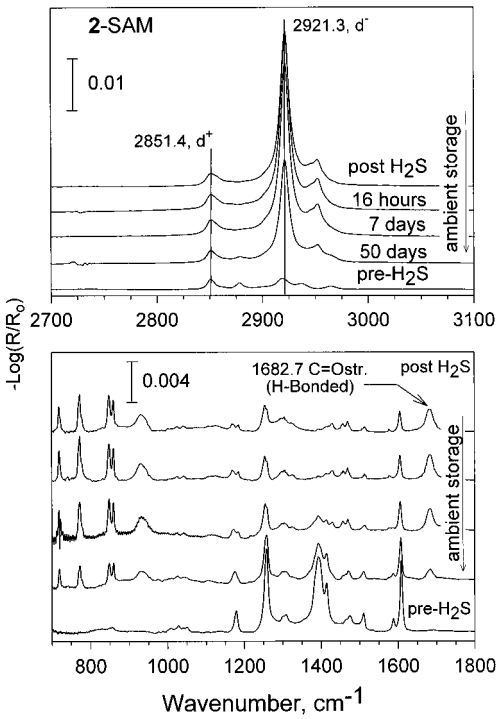

Figure 6. 6. IRS spectra of a **2**-SAM on Ag. The spectra were taken before and after exposure to H_2S, as indicated.

2 times larger. We ascribe this apparent contradiction to the use of optical functions from the CO_2H form of **2** rather than the more appropriate CO_2^- salt (the latter could not be prepared in a well-crystallized form). Unlike the case of alkanoic acids, where the optical functions for the alkyl chains are quite similar for the salts and acid forms, it appears that some of the ring mode intensities are perturbed by the *p*-CO_2^- group. On this basis we set the ring plane orthogonal to the surface using the

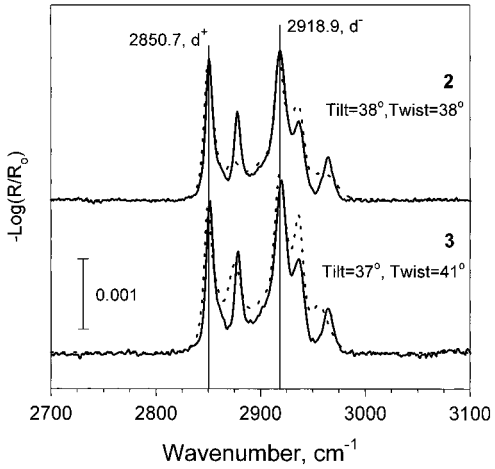

Figure 7. 7. IRS spectra of the initial **2**- and **3**-SAMs in the C−H stretching region. The dotted lines are best-fit simulated spectra using the optical function spectra of the bulk, polycrystalline acids (*k* spectra given in Figure 5).

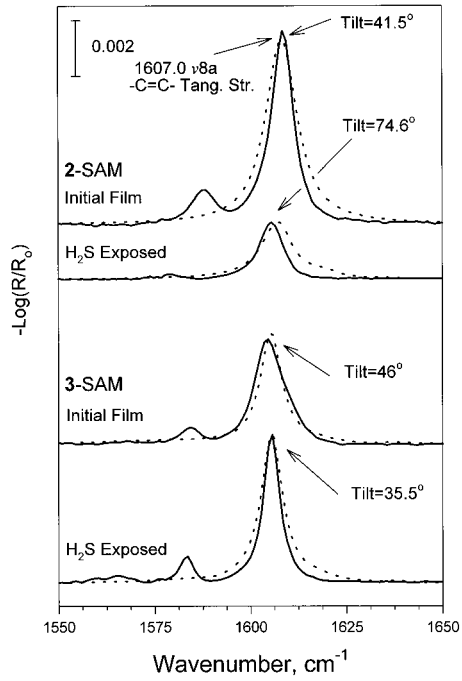

Figure 8. Experimental (solid line) and best-fit simulated (dotted line) IRS spectra for the ν_{8b} (−C═C− tangential) stretch of the initial and H_2S-exposed **2**- and **3**-SAMs.

more reliable criterion of the missing ν_1 and ν_{17b} intensities. This geometry is quite consistent with the CO_2^- group spectra (see above).

In Figure 7, the d^+, d^- peak positions at 2851 and 2919 cm^{-1}, respectively, are slightly higher than the values of 2849 and 2916 cm^{-1} observed for the initial **1**-SAM and indicate that while the **2**-SAM chains are predominantly all-trans, they contain a slightly higher gauche defect content than the **1**-SAM chains. Using the measured ellipsometric thickness of 22 ± 1 Å, a best-fit simulation analysis was performed using the optical function spectra (Figure 5). The result for the d^+ and d^- modes, shown in Figure 7, gives an alkyl chain tilt of ∼38 ± 1° with a ∼38 ± 2° chain twist. The lower quality of the fit for the CH_3 stretching mode groups is likely due to some localized disorder near the chain termini where gauche defects will be concentrated.

Combining the above data leads to an overall average initial SAM structure as illustrated in Figure 4, where the 1,4 aromatic

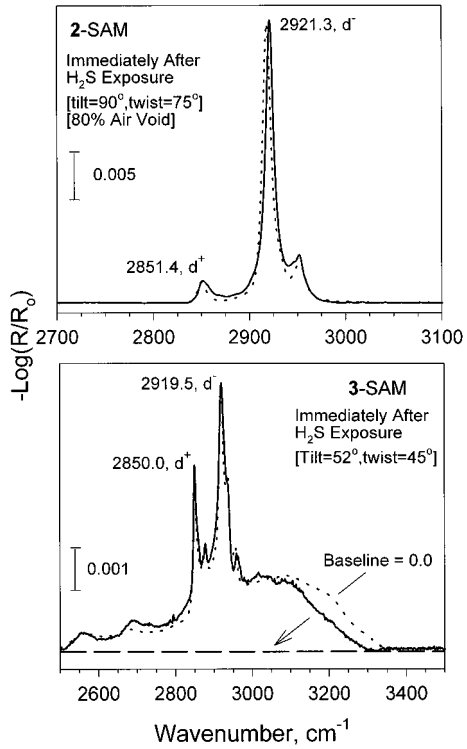

Figure 9. 9. IRS spectra of the **2**- and **3**-SAMs in the C−H stretching region immediately after H_2S exposure. The dotted lines are best-fit simulated spectra using the optical function spectra of the bulk, polycrystalline acids (*k* spectra given in Figure 5).

axis, collinear with the C_{AR}−O ether bond, is assigned a zero tilt. Setting the $C_{AR}O-CH_2$ bond rotation angle α to zero (all-trans chain, see Figure 3B) and assuming approximate values of ∼110−112° for the C−O−C and C−C−C bond angles[25] give $\theta_{CHAIN} \approx 35°$, quite close to the experimentally deduced value. Consistent with this value, the rotation angle β can assume any value. We note that this structure is somewhat idealized since the d^+ and d^- peak positions (see above) suggest the presence of occasional gauche defects in the chains relative to the **1**-SAM.

3.2.2. Post-H_2S, Immediate Analysis. Upon exposure the water contact angle drops from 110° to ∼90°, while the hexadecane value drops from 52° to near zero. These results are similar to those of the **1**-SAM and indicate a change from a CH_3 surface to that similar to a CH_2 one.

The IR spectra taken at various intervals after H_2S exposure are given in Figure 6. The most significant observation is that immediately after exposure ν_s (CO_2^-), near 1394 cm^{-1} initially, disappears while the C═O stretching mode of the hydrogen-bonded CO_2H dimer ring[26] ($\nu_{C=O}^{dimer}$) appears at 1683 cm^{-1}, an indication that the original interface has been broken.

From the high frequency region spectrum, shown in detail in Figure 9 (top), three important conclusions are drawn. First, the absence of the broad ν_{OH}^{dimer} band, normally a strong feature[27] near 2800−3300 cm^{-1}, as seen in Figure 3 (top), places the dimer ring axis nearly parallel to the substrate plane, based on the assignment of **p** in the plane of the dimer ring.[28] Assuming coplanarity of the aromatic and CO_2H dimer rings, then the aromatic rings also will lie similarly parallel to the surface. Second, based on the negligible shifts in the d^+ and d^- peak locations relative to the pre-exposed SAM, the conformational chain order appears to be maintained, although a slight (∼25%) peak broadening does suggest some increase in gauche defects. Third, the contrasting large change in the *intensities* of d^+ and d^- modes indicates a major change in the

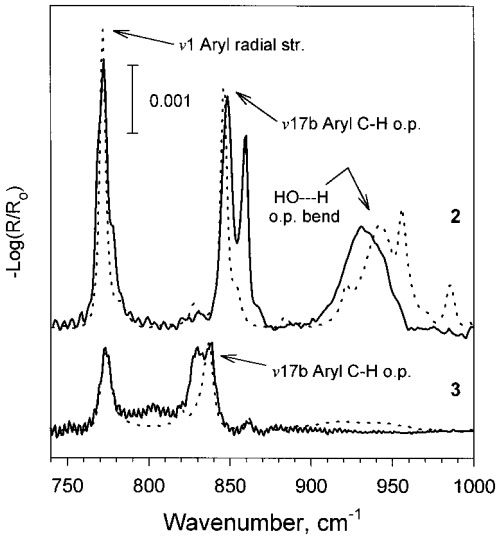

Figure 10. Low-frequency region IRS spectra for the **2**- and **3**-SAMs immediately after H_2S exposure. The dotted lines are best-fit simulated spectra using the optical function spectra of the bulk, polycrystalline acids (*k* spectra given in Figure 5).

average chain *orientation* (compare Figure 9 to Figure 7, top) occurs upon exposure. A number of simulations led to the conclusion that good fits to experiment can be obtained only with the discrete crystallite model, as for the **1**-SAM case. The best fit is shown in Figure 9 (top) and corresponds to a chain tilt and twist of ∼90° and 75 ± 2°, respectively, with a final void content of 80 ± 5%, which in the ideal case of uniform size crystallites would give ∼130 Å particles. This geometry places the alkyl chain axes parallel to the surface but with a slight (∼15°) twist of the C−C−C plane away from the surface. We caution that the crystallite size represents an average value with no indication of the size dispersion nor shape. The results are summarized in Table 2.

Using the best-fit model deduced in the C−H mode analysis, which locks in the alkyl chain geometry and the requirement of a discrete crystallite film model, the average tilt of the 1,4 para-axis of the aromatic ring can be calculated using the ν_{8a} −C═C− tangential stretching mode (**p** parallel to the 1,4 axis) intensity in Figure 8. In this case, in contrast to the initial carboxylate **2**-SAM case, we presume that the optical function spectra accurately represent the film optical response since the acid dimer form of **2** exists in both bulk and film states. This analysis (Figure 8) results in a ∼75° tilt of the 1,4 axis. This places the long axis phenyl ring nearly parallel to the substrate, in agreement with the parallel alignment of the long axis of the hydrocarbon chains determined above.

The lower 750−1000 cm^{-1} region was also analyzed in this manner, and the results are shown in detail in Figure 10. The diagnostic ν_1 and ν_{17b} modes, absent initially, appear after H_2S exposure. These modes, with **p** along the radial axis and out-of-plane, respectively, were analyzed to reveal the rotation of the phenyl ring around the 1,4 (tangential or long) axis of the molecule. Since the tilt of this axis was set above by the ν_{8a} mode intensity, the only free parameter is the twist ψ which regulates the intensities of the ν_1 and ν_{17b} modes. The resulting best fit, shown in Figure 10 (dotted line), based on a model with θ(ring) set at 75° (from the ν_{8a} fit in Figure 8, see above), represents a twist of $\psi = 32 \pm 4°$, which places the ring planes significantly rotated away from the surface plane (refer to Figure 3A). The latter implies a preference for the crystallites to orient with the aromatic rings toward an "edge-on", overlapped fashion across the surface, as opposed to the ring planes stacked parallel to the surface.

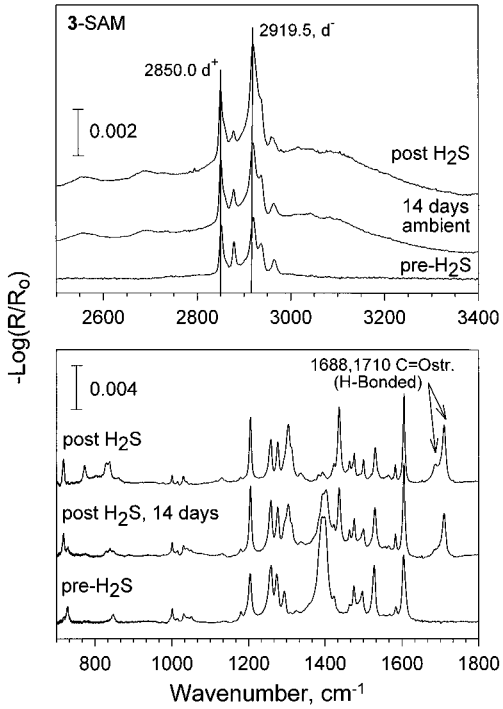

Figure 11. IRS spectra of a **3**-SAM on Ag. The spectra were taken before and after exposure to H_2S, as indicated.

The self-consistency of the above structure can be confirmed from analysis of the out-of-plane bending CO_2H dimer ring (γ_{OP}^{dimer}) mode, near 942 cm^{-1}. Application of the discrete crystallite model gives a best-fit dimer ring twist of a 32 ± 4° (Figure 10, top). With the assumption of coplanarity of the aromatic and dimer rings, this value is in excellent agreement with the aromatic ring orientation deduced above. Summaries of the deduced molecular orientations are given in Table 1 and Figure 4.

3.2.3. Post H_2S, Extended Ambient Exposure. Interestingly, only slight changes in the reorganized film spectra were observed with extended ambient exposure (Figure 6), even after 50 days. Since the initial reorganization process is immediate upon H_2S treatment, leaving a surface with a large extent of void regions exposed to air for facile re-establishment of the surface oxide, the slow reverse process must reflect the high thermodynamic stability of the reorganized film structure relative to that of the **1**-SAM, which reverses within a few days.

3.3. The 4-Hexadecyloxybiphenyl-4′-carboxylic Acid (3) SAM. *3.3.1. Pre-H_2S Structure.* The initial SAM shows a general structure quite similar to that of the corresponding **2**-SAM. The ellipsometric thickness is 28 ± 1 Å, and the water and hexadecane contact angles are 110 ± 2° and 52 ± 2°, respectively. The IR spectra are given in Figures 7, 8, 10, and 11. From Figure 11 (bottom), the strong ν_s (CO_2^-) peak and the apparent absence of a ν_a (CO_2^-) feature again indicates a symmetrical bidentate type of CO_2^- headgroup attachment. The close similarity of the d^+ and d^- spectra for the **2**- and **3**-SAMs, shown together in Figure 7, indicates that the alkyl chains have near identical structures in the two monolayers. Simulation analysis of the C−H stretching mode spectra using the bulk **3** optical functions (Figure 5) gives a chain tilt and twist of 37 ± 1° and 41 ± 2°, respectively. The results are summarized in Table 2. For the reasons given earlier (see section 3.2.1), the aromatic modes of bulk phase **3** were not applied to a spectral simulation analysis of the initial SAM. However, one can qualitatively note that the near absence of the ν_1 and ν_{17b} modes (700−1100 cm^{-1} region, Figure 11 bottom) in the pre-H_2S spectra supports the orthogonal placement of the aromatic rings

suggested by the CO_2^- headgroup attachment. The average structure of the molecules in the **3**-SAM is depicted in Figure 4.

3.3.2. Post-H_2S, Immediate Analysis. Exposure of the **3**-SAM to H_2S results in quite different structural changes than with the other SAMs. The simplest demonstration of this is that the water and hexadecane contact angles drop by only 10° and ~15°, respectively, to leave a surface remaining both quite hydrophobic and oleophobic. However, H_2S does break the film interface and convert the CO_2^- headgroups to CO_2H species, as seen in the spectra in Figure 11 which show no evidence of CO_2^- modes but do show the appearance of the $\nu_{C=O}^{dimer}$ mode as bands at 1688 and 1710 cm^{-1}.

Inspection of the C−H stretching mode spectra (Figure 11, top) shows only small perturbation of the alkyl chains from H_2S exposure, with the major changes being only slight frequency decreases of 1.4 and 0.7 cm^{-1} and slight intensity increases of ~1.6 and 1.8 for the d^+ and d^- modes, respectively. In comparison, the d^+ and d^- modes of the **2**-SAM increase by factors of ~1.2 and ~14, respectively (Figure 6). The frequency shifts indicate an increase in the chain conformational order, but the final frequencies of 2850.1 and 2919.5 cm^{-1} still reflect the presence of some gauche defects, relative to those for the chains in the initial **1**-SAM. Evidence for a crystalline packing with an orthorhombic subcell is given by the doublet splitting of the γ_{CH_2} mode at 1464 and 1476 cm^{-1}.[29]

A variety of C−H stretching mode simulation models were explored. Good fits were obtained using uniform density models, in contrast to the **1**- and **2**-SAM cases, where island models were required. The best-fit model (Figure 9, bottom) gives a chain tilt and twist of 52 ± 2° and 45 ± 2°. The latter value is consistent with an orthorhombic subcell, indicated by the γ_{CH_2} splitting, in which the two subcell chains with planes set orthogonal would give a constant average twist value of 45°. The chain tilt is greater than the initial tilt of 37° (Figure 7). The chain tilt increase and the overall increase in chain organization are consistent with the contact angle data, which show only small decreases in the hydrophobicity and oleophobicity. One should note that an increased tilt angle structure, which increases the area per chain, implies that some molecules must be moved out of the original film layer. This would give some degree of molecular scale roughening and thus give rise to a more corrugated surface with consequent increased exposure at the wetting surface of CH_2 units. This conclusion is quite consistent with the small drop in water and hexadecane contact angles upon H_2S exposure.

Figure 11 (top) shows a very broad feature over the range 2400−3300 cm^{-1}, with a maximum near 3100 cm^{-1} and two smaller adsorptions near 2557 and 2687 cm^{-1}. The broad peak at 3100 cm^{-1} is attributed to be the center of the ν(OH) stretching mode, and the smaller peaks are combination bands which include the ν(OH) and ν(C−O) stretches.[30] These combination bands, which are typically not observed in *n*-alkanoic acids in the crystalline or solution state,[27,28] are observed in the bulk spectra of molecules **2** and **3** (Figure 5). It has also been shown that these combination bands are most prominent for $-CO_2H$ groups in a linear, polymeric hydrogen-bonded state such as that obtained for crystalline formic acidic.[31] The calculated spectrum (Figure 9 bottom, dotted line) includes the O−H stretching absorption and assumes that the entire O-H band arises from stretching vibrations polarized along the (OH---O) linkage (ν_{OH}^{poly}). The calculated spectrum shown represents a 36 ± 4° tilt of the (OH---O) linkage from the surface normal. We note that these simulations are approximate since the intensities of O−H stretching vibrations can vary significantly with the exact extent of H-bonding interactions. In our simulations the O−H intensities are represented by those of the bulk-phase material and thus may contain a different distribution of H-bonding states, although one can note that the same general broad types of spectral distributions are present in both the *k* spectrum (Figure 5) and the H_2S-exposed SAM (Figure 9) spectrum. One should also note that assumption of an isotropic distribution of H-bond directions gives a simulated intensity that is too small by a factor of 2. This observation together with the presence of two components to the $\nu_{C=O}^{dimer}$ mode and the absence of a strong γ_{OP}^{dimer} mode near 942 cm^{-1} (region shown in Figure 10) is an indication of several hydrogen-bonding configurations, which include the linear polymeric hydrogen-bonding network.

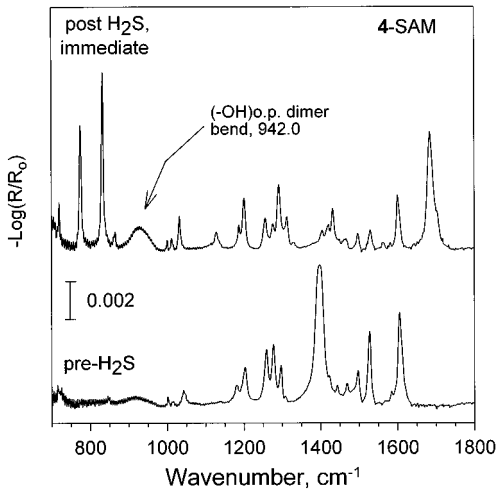

Figure 12. IRS spectra of a 4-methoxybiphenyl-4′-carboxylic acid (**4**)/Ag SAM (note the absence of an alkoxy group). The spectra were taken before and after exposure to H_2S, as indicated.

Analysis of the ν_{8a}, ν_{17b}, and ν_1 modes was made to determine the biphenyl ring orientations. The ν_{8a} mode result gives a best-fit tilt of $\theta = 35.5 \pm 2°$ for the long (tangential) ring axis (fit shown in Figure 8). Analysis of ν_{17b} and ν_1 modes (Figure 10, bottom) gives a best-fit ring twist of $\psi = 36 \pm 2°$. The ring orientations are summarized in Table 2 and shown in Figure 4. To arrive at an average molecular structure that is consistent with these ring orientations and the alkyl chain orientations deduced above, it is also necessary to rotate the chain out of the *xz*-plane (page in Figure 4). This could be accomplished by variations in the chain rotation angle β (and α or as well, Figure 3B), and it is not possible to define a unique structure from the data. In addition, since the γ_{CH_2} mode indicates two chains per unit subcell, the picture is even more complex. Thus the picture in Figure 4 carries only the essential features.

All the above observations lead to a picture of the H_2S-exposed film in which the nascent CO_2H headgroups remain in physical contact (physisorbed) with the substrate and form a quasi-two-dimensional hydrogen-bonded network which continues to uniformly cover or wet the surface. Since this behavior is so distinctly different from the substrate-dewetting behavior of the **1**- and **2**-SAMs, with no and one constituent phenyl ring in the molecule, respectively, the role of the additional phenyl ring in the **3**-SAM behavior was examined further. For this purpose, a SAM was formed from the acid $HO_2C-C_6H_4-C_6H_4-OCH_3$ (**4**), which contains no alkyl tail to stabilize the SAM. The spectrum of the SAM is shown in Figure 12. In contrast to the **3** case, the appearance of a strong γ_{OP}^{dimer} mode near 942 cm^{-1} and the very intense ν_1 and ν_{17b} modes near 776 and 833 cm^{-1}, respectively, clearly demonstrate that absence of the alkyl chain redirects the H_2S-induced reorganization back

to the type observed with the **1**- and **2**-SAMs, where crystallites of bulk-phase acid dimer are formed.

3.3.3. Post H_2S, Extended Ambient Exposure. Similar to the **2**-SAM case, the return of the H_2S-exposed SAM structure to the original form during ambient storage was extremely slow. Only minimal changes in the IR spectra were observed over several weeks exposure to the ambient atmosphere (Figure 11). As with the **2**-SAM, this effect must be due to the inherently stable film structure since even the inherently wellformed initial SAM is quite permeable to H_2S gas, so the reorganized film, which is similarly dense, must be permeable to O2 and thus not be rate limiting for the oxidative degradation of the substrate sulfide layer.

4. Discussion and Conclusions

In summary, we have reported the effects of strong, sudden perturbation of the monolayer−substrate interface by interaction with H_2S vapor for a series of straight chain and liquid crystalline carboxylic acid self-assembled monolayers. All the initial SAM films are anchored by a symmetrical $-CO_2^-$ ligand species formed through dissociative chemisorption of the acid at the ambient oxide of a silver substrate. The $-CO_2^-$ $|Ag^+$ interaction is quite strong, with an estimated a bond energy of ∼33 kcal/mol.[16] In all cases, brief exposure to H_2S gas causes sulfidation of the Ag surface[9,10] with a sudden destabilization of the interface via loss of the strong $-CO_2^-|Ag^+$ interaction, conversion of the CO_2^- to CO_2H species, and rapid reorganization of the film. The protonation of the CO_2^- group by H_2S, a far weaker acid than those of the carboxylic acids in this study by ∼5−6 pK_a units [p$K_a(H_2S) = 11.96$[25]], is obviously driven by the large exothermic ΔH for the formation of highly insoluble Ag−S at the surface.[10,25] However, two distinctly different film reconstruction pathways, which depend upon the intrinsic chemical structure of the constituent film molecule, result upon the exothermic breaking of the SAM interface.

The aromatic carboxylic acid molecules in this study both possess much larger intermolecular attractions than **1**, as is qualitatively evident from the observed melting points of 62.8, 132.5, and 236.9 °C for **1**, **2**, and **3**, respectively. In the cases of SAMs of **1** and **2**, H_2S causes a dewetting behavior with breakup into dispersed crystallites of the initial acid. This observation shows that, in the absence of the CO_2^- $|Ag^+$ interaction, the bulk crystalline forms of these acids, stabilized somewhat by the formation of CO_2H dimers with interaction energies of ∼12.5 kcal/mol,[32] are thermochemically more favorable than a uniform monolayer. In strong contrast, in the case of the 4′-hexadecyloxybiphenyl group (**3**) SAM, H_2S disruption of the CO_2^- $|Ag^+$ interface forms CO_2H groups, but the constituent molecular units remain locked in place, uniformly distributed across the surface, with the CO_2H groups physisorbed and stabilized in the form of a quasi-two-dimensional hydrogen-bonded network at the substrate. Further, since the substitution of the $C_{16}H_{33}O$ tail for a simple CH_3O group leads to the dewetting pathway, one can conclude that the biphenyl group by itself has no special role in the stabilization against dewetting.

From these data it appears that the wetting/dewetting competition is directly affected by the total intermolecular interaction energy (the cohesive energy density) of the film constituent molecules. The question arises as to whether these effects are equilibrium or thermodynamic in nature or kinetic. It is certainly clear that this uniform network structure is quite stable (for weeks at ambient temperature), and if the effect is kinetic, then the relatively high activation barrier for dewetting must reflect this stability.

Acknowledgment. Financial support from National Science Council, Republic of China (Y.T. and W.L.), and the National Science Foundation (G. H.) is gratefully acknowledged.

References and Notes

(1) (a) Swalen, J. D.; Allara, D. L.; Andrade, J. D.; Chandross, E. A.; Garoff, S.; Israelachvili, J.; McCarthy, T. J.; Murry, R.; Pease, R. F.; Rabolt, J. F.; Wynne, K. J.; Yu, H. *Langmuir* **1987**, *3*, 932−950.

(2) Tao, Y. T.; Hietpas, G. D.; Allara, D. L. *J. Am. Chem. Soc.* **1996**, *118*, 6724−6735.

(3) McDermott, M. T.; Green, J. B. D.; Porter, M. D. *Langmuir* **1997**, *13*, 2504−2510. Roundtree, P.; Dugal, P. C.; Hunting, D.; Sanche, L. *J. Phys. Chem.* **1996**, *100*, 4546−4550. Schlenoff, J. B.; Li, M.; Ly, H. *J. Am. Chem. Soc.* **1995**, *117*, 12528−12536.

(4) Xia, Y.; Whitesides, G. M. *Langmuir* **1997**, *13*, 2059−2067. Lercel, M. J.; Redinbo, G. F.; Pardo, F. D.; Rooks, M.; Tiberio, R. C.; Simpson, P.; Sheen, C. W.; Parikh, A. N.; Allara, D. L. *J. Vac. Sci. Technol.* **1994**, *B12*, 3663−3667. Huang, J.; Hemminger, J. C. *J. Am. Chem. Soc.* **1993**, *115*, 3342−3343.

(5) Braun, F. N.; Sluckin, T. J.; Velasco, E. J. *Phys. Condens. Matter* **1996**, *8*, 2741−2754.

(6) Bahadur, B. *Liquid Crystals; Applications and Uses;* World Scientific Publishing: Singapore, 1992; Vol. 3. Chandrasekhar, S. *Liquid Crystals,* 2nd ed.; Cambridge University Press: Cambridge, 1992.

(7) Reference 2 and Schlotter, N. E.; Porter, M. D.; Bright, T. B.; Allara, D. L. *Chem. Phys. Lett.* **1986**, *132*, 93−98.

(8) Tao, Y. T. *J. Am. Chem. Soc.* **1993**, *115*, 9547−9555.

(9) Bennett, H. E.; Peck, R. L.; Burge, D. K.; Bennett, J. M. *J. Appl. Phys.* **1969**, *40* (8), 3351−3360. Rice, D. W.; Peterson, P.; Rigby, E. B.; Phipps, P. B. P.; Cappell, R. J.; Tremoureux, R. *J. Electrochem. Soc.* **1981**, *128* (2), 275−284. Graedel, T. E.; Franey, J. P.; Gualtieri, G. J.; Kammlott, G. W.; Malm, D. L. *Corros. Sci.* **1985**, *25* (12), 1163−1180.

(10) Graedel, T. E. *J. Electrochem. Soc.* **1992**, *139* (7), 1963−1970.

(11) Gray, G. W.; Hartley, J. B.; Jones, B. J. *J. Chem. Soc.* **1955**, *236*, 1312−1420.

(12) Barr, M. R.; Dunell, B. A.; Grant, R. F. *Can. J. Chem.* **1963**, *41*, 1189−1196.

(13) Laibinis, P. E.; Whitesides, G. M.; Allara, D. L.; Tao, Y. T.; Parikh, A. N.; Nuzzo, R.G. *J. Am. Chem. Soc.* **1991**, *113*, 7152−7167.

(14) Parikh, A. N.; Allara, D. L. *J. Chem. Phys.* **1992**, *96*, 927−945.

(15) Sondag, A. H. M.; Raas, M. C. *Appl. Spectrosc.* **1989**, *43* (1), 107−113.

(16) Canning, N. D. S.; Madix, R. J. J. *Phys. Chem.* **1984**, *88*, 2437−2446.

(17) Further, if the structure is orthorhombic with two chains per unit subcell, as suggested previously by Schlotter et al.,[7] it is likely that there are two types of CO_2^- configurations as well as the presence of a gauche kink near the headgroup of the chain, a possibility earlier suggested for the structure of Langmuir−Blodgett films of cadmium eicosonoate [Allara, D. L.; Swalen, J. D. *J. Phys. Chem.* **1982**, *86*, 2700].

(18) Smith, E. L.; Porter, M. D. *J. Phys. Chem.* **1993**, *97*, 8032−8038.

(19) Solution adsorption experiments were carried out using 1 mM THF solutions.

(20) The entire complex optical function spectrum is available in tabular form from the authors (D. L. Allara) upon request.

(21) Young, J. T.; Tsai, W. H.; Boerio, F. J. *Macromolecules* **1992**, *25*, 887−894.

(22) Varsanyi, G. *Vibrational Spectra of Benzene Derivatives;* Academic Press: New York, 1974.

(23) This mode could alternatively be the ν_{12} mode, which has the same direction of **p** (ref 22).

(24) Tobin, M. *J. Phys. Chem.* **1957**, *61*, 1392−1400.

(25) *CRC-Handbook of Chemistry and Physics*, 73rd ed.; CRC Press: Boca Raton, 1992−1993.

(26) Hayashi, S.; Umemura, J. *J. Chem. Phys.* **1975**, *63* (5), 1732−1740.

(27) Sinclair, R. G.; McKay, A. F.; Jones, R. N. *J. Am. Chem. Soc.* **1952**, *74*, 2570−2575. Bratoz, S.; Hadzi, D.; Sheppard, N. *Spectrochim. Acta.* **1956**, *8*, 249−261.

(28) Susi, H. *J. Am. Chem. Soc.* **1959**, *81*, 1535−1540.

(29) Snyder, R. G. *J. Mol. Spectrosc.* **1961**, *7*, 116−144.

(30) Teragni, P.; Masetti, G.; Zerbi, G. *Chem. Phys.* **1978**, *28*, 55−72.

(31) Raval, R.; Munro, S. *J. Electron. Spectrosc. Relat. Phenom.* **1993**, *64/65*, 461−468. Millikan, R. C.; Pitzer, K. S. *J. Am. Chem. Soc.* **1958**, *80*, 3515−3521.

(32) Herzberg, G. *Molecular Spectra and Molecular Structure II,* 1st ed.; Van Nostrand Reinhold Inc.: New York, 1945; p 536.